forum acusticum 2026
8-12 September · Graz, Austria

# A ROBUST ADAPTIVE WAVENUMBER SAMPLING APPROACH FOR EFFICIENT 2.5D ACOUSTIC SIMULATIONS

Likun Luo[1], Florian Toth[1]

[1] *Institute of Mechanics and Mechatronics, TU Wien, Austria*

This paper is a revised version of the authors' submitted manuscript that was peer-reviewed by at least two anonymous reviewers.



## Abstract

The 2.5D acoustic finite and boundary element methods efficiently solve wave propagation problems for longitudinally invariant geometries by employing a wavenumber decomposition in the invariant direction. However, evaluating the improper Fourier integral across the wavenumber spectrum remains a significant computational challenge, as it relies on the numerical integration of a continuous spectrum resolved via discrete sampling strategies. While adaptive sampling schemes reduce the number of required 2D calculations, existing methods relying on purely local relative errors experience numerical instability when the spectral amplitudes approach zero. Furthermore, standard numerical quadrature struggles with the highly oscillatory inverse Fourier kernel, introducing additional integration errors. This paper proposes a robust adaptive wavenumber sampling approach that approximates the spectrum using strictly piecewise linear segments. This deliberate geometric restriction enables the exact analytical evaluation of the oscillatory integral via Filon-type quadrature, effectively eliminating numerical integration errors. To drive the sampling scheme, a hybrid local error norm is introduced to ensure stability near zero, combined with a global convergence check on the physical spatial pressure. Numerical examples demonstrate that the proposed approach drastically reduces computational effort while maintaining the strict accuracy of dense equidistant sampling.

**Keywords:** *2.5d acoustics, wavenumber-domain method, finite element method, adaptive sampling, filon-type quadrature*

## 1. Introduction

The 2.5D finite and boundary element methods have emerged as highly efficient techniques for predicting wave propagation and environmental noise around longitudinally invariant structures, such as railway tracks, tunnels, and noise barriers [1], [2]. By leveraging the assumption of invariant geometry and material properties along the axis of wave propagation, the 2.5D approach elegantly reduces a computationally demanding 3D spatial problem into a series of highly manageable 2D cross-sectional problems solved in the frequency-wavenumber domain.

Despite this geometric simplification, the method introduces a significant computational bottleneck: the evaluation of the spatial Fourier transform. To obtain the physical spatial pressure distribution, the 2D wave equation must be solved across a wide spectrum of longitudinal wavenumbers, which must subsequently be integrated. Because this represents an improper integral containing a highly oscillatory exponential kernel, traditional numerical quadrature relying on fixed, equidistant wavenumber sampling demands excessively high resolution. This forces the evaluation of thousands of 2D problems, drastically increasing computation time.

To address this computational burden, adaptive wavenumber sampling schemes have been proposed. Notably, Park et al.[3] recently introduced a valuable iterative convergence scheme that reduces the number of calculated wavenumbers by evaluating the relative difference between simultaneous linear and spline interpolations, refining the sampling only where the difference exceeds a threshold. We build on the idea of Park et al., addressing some limitations like the relative error norm, the perhaps unecessarly high order of the spline interpolation and the quadrature not adapted to the oscillatory kernel. To overcome these limitations and maximize computational efficiency, this paper proposes a robust adaptive wavenumber sampling approach. This methodology deliberately restricts the spectral approximation to purely piecewise linear segments. This deliberate restriction not only streamlines adaptive node insertion but uniquely enables the exact analytical integration of the highly oscillatory inverse Fourier kernel via Filon-type quadrature, effectively

***Corresponding author:*** *likun.luo@tuwien.ac.at.*

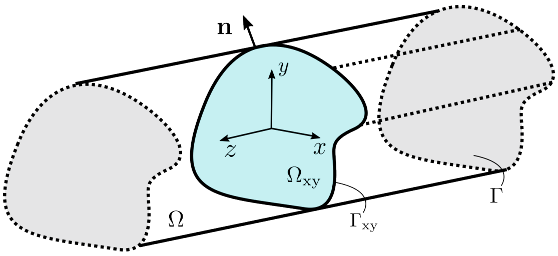


**Figure 1:** Simple sketch of an infinite acoustic domain $\Omega$ with uniform geometry and properties in the $z$ direction, where $\Gamma$ is the outer surface. $\Omega_{\mathrm{xy}}$ is the cross-section area and $\Gamma_{\mathrm{xy}}$ is the cross-section perimeter. Both the domain $\Omega$ and $\Omega_{\mathrm{xy}}$ share the same outer normal vector $\mathbf{n}$.

eliminating numerical integration errors in the final spatial transformation. To ensure rigorous geometric approximation without numerical breakdown near zero, a hybrid local error norm is introduced to drive the sampling scheme. Finally, a physics-driven global convergence check guarantees that the algorithm terminates precisely when the spatial pressure at the receiver location converges.

## 2. Helmholtz Equation in 2.5D

The governing equation for a linear acoustic problem in the frequency domain is the Helmholtz equation

$$\nabla^2 p\,(x,y,z) + k^2 p\,(x,y,z) = q\,, \tag{1}$$

where $p$ is the complex-valued acoustic pressure in the spatial domain and $\nabla^2 = \frac{\partial^2}{\partial x^2} + \frac{\partial^2}{\partial y^2} + \frac{\partial^2}{\partial z^2}$ denotes the 3D Laplacian operator. The scalar wavenumber $k$ is defined by the dispersion relation

$$k^2 = \|\mathbf{k}\|_2^2 = k_x^2 + k_y^2 + k_z^2 = \frac{\omega_{\mathrm{3D}}^2}{c_0^2}\,, \tag{2}$$

where $\omega_{\mathrm{3D}}$ is the angular frequency of the three-dimensional Helmholtz equation, $c_0$ is the adiabatic speed of sound in the fluid medium, and $\mathbf{k} = [k_x, k_y, k_z]^\top$ is the three-dimensional wave vector. The known source field is denoted $q$.

For acoustic domains exhibiting geometric invariance and constant material properties along the longitudinal (z-)axis, as shown in Fig. 1, the three-dimensional spatial pressure field can be efficiently decomposed into a set of independent subproblems in the wavenumber domain. This transformation utilises the Fourier transform pair over $z$:

$$\tilde{p}\,(x,y,k_z) = \int_{-\infty}^{\infty} p\,(x,y,z)\,e^{ik_z z}\mathrm{d}z\,, \tag{3}$$

$$p\,(x,y,z) = \frac{1}{2\pi}\int_{-\infty}^{\infty} \tilde{p}\,(x,y,k_z)\,e^{-ik_z z}\mathrm{d}k_z\,. \tag{4}$$

Applying this transformation to Eq. (1) yields the Helmholtz equation in the wavenumber domain

$$\nabla_{\mathrm{xy}}^2\,\tilde{p}\,(x,y,k_z) + \left(\frac{\omega_{\mathrm{3D}}^2}{c_0^2} - k_z^2\right)\tilde{p}\,(x,y,k_z) = \tilde{q}\,, \tag{5}$$

where $\nabla_{\mathrm{xy}}^2 = \frac{\partial^2}{\partial x^2} + \frac{\partial^2}{\partial y^2}$ denotes the 2D Laplacian operator. The unknown $\tilde{p}$ represents the wavenumber-domain pressure associated with a specific axial wavnumber $k_z$. To reconstruct the 3D acoustic pressure field, Eq. (5) is solved for a discrete set of wavenumbers, and the inverse Fourier transform is subsequently applied according to Eq. (4).

### 2.1. Monopole point source

The excitation is modelled as a monopole point source located at $\mathbf{x_0} = [x_0, y_0, z_0]^\top$. Consequently, the right-hand side of Eq. (1) reads $q = -i\omega_{\mathrm{3D}}\rho_0 Q\delta\,(\mathbf{x} - \mathbf{x_0})$, where $\rho_0$ is the medium fluid density, $Q$ denotes the volume velocity and $\delta$ the Dirac-delta function.

Applying the forward Fourier transform along the $z$-direction, the source term in Eq. (5) becomes $\tilde{q} = -i\omega_{\mathrm{3D}}\rho_0 Q\delta\,(x - x_0)\,\delta\,(y - y_0)\,e^{ik_z z_0}$. Since the geometry and material properties are invariant along $z$, the source may be placed at $z_0 = 0$ without loss of generality. The phase factor $e^{ik_z z_0}$ then reduces to unity and the transformed source term is independent of the axial wavenumber $k_z$, meaning the excitation magnitude remains constant for each 2D subproblem across the wavenumber spectrum.

## 3. Adaptive Wavenumber Sampling

The computation of the physical pressure field requires evaluating the infinite integral of the continuous wave number spectrum in Eq. (4). In practice, the integration limits are truncated at the wavenumber associated to the excitation angular frequency $k_{z,\mathrm{exci}} = \omega_{\mathrm{3D}}/c_0$, or slightly beyond by adding a small offset $(k_{z,\mathrm{exci}} + k_{z,\mathrm{offset}})$. This truncation is justified by the physical properties of the spectrum, which exhibits rapid amplitude decay in the evanescent region where $k_z > k_{z,\mathrm{exci}}$. The primary challenge lies in efficiently discretising the continuous spectrum. A conventional approach utilises equidistant sampling with a fixed step size $\Delta k_z$, as proposed by Duhamel [4]. However, this strategy is inherently limited as it fails to account for the local features of the wavenumber spectrum. In railway acoustic free-field problems, for instance, the vehicle carbody acts as a significant scatterer. In such cases, the spectrum is characterised by distinct peaks corresponding to acoustic reflections and singularities near the excitation wavenumber $k_{z,\mathrm{exci}}$. Between these localised high-energy regions, the spectral amplitude is often negligible because the spatial solution is the integral of the spectrum. Park et al.[3] identified these spectral characteristics in the context of structural vibration problems and proposed an initial adaptive sampling strategy which we will extend in the following Sections 3.1 through 3.4, with the final robust algorithm summarised in Section 3.5.

### 3.1. Piecewise linear approximation

The continuous wavenumber spectrum $\tilde{p}\,(k_z)$ is approximated by a series of local, piecewise linear elements. Thus, we obtain $\tilde{p}(k_z)$ by solving Eq. (5) at a set of wave numbers $k_{z,i}$ and linearly interpolate in between. This linear approach is selected for its high flexibility within the adaptive refinement framework. Unlike higher-order spline interpolations, linear segments allow straightforward insertion of new control points without affecting neighbouring intervals or requiring global recomputation. Furthermore, the simplicity of the linear basis function is critical for the analytical integration of the oscillatory kernel in the subsequent Filon-type quadrature (Section 3.4). While splines could provide higher smoothness, they would significantly increase the complexity of the analytical segment solutions and the dynamic management of the sampling grid.

### 3.2. Hybrid local error metric

To determine if a wavenumber interval $[k_{z,i}, k_{z,i+1}]$ with width $\Delta k_{z,i}$ requires further refinement, a hybrid local error metric $\epsilon_{\text{local},i}$ is evaluated at the interval midpoint $k_{z,\text{m},i} = k_{z,i} + \frac{\Delta k_{z,i}}{2}$, which yields

$$\epsilon_{\text{tol,local},i} = \underbrace{\frac{\|\tilde{p}_{\text{linear},i}\left(k_{z,\text{m},i}\right) - \tilde{p}_{\text{true}}\left(k_{z,\text{m},i}\right)\|_2}{\|\tilde{p}_{\text{true}}\left(k_{z,\text{m},i}\right)\|_2}}_{\epsilon_{\text{tol,rel},i}} + \epsilon_{\text{tol,abs}} \,. \tag{6}$$

Here, $\tilde{p}_{\text{true}}$ represents the numerical solution obtained from the FE/BE solver.

To ensure the algorithm is robust against numerical noise in low-amplitude regions, the absolute tolerance $\epsilon_{\text{tol,abs}}$ is not a fixed constant. Instead, it is dynamically scaled to the global maximum of the spectrum and reads as

$$\epsilon_{\text{tol,abs}} = \max\left(\alpha \cdot \max_{k_z}\left(\|\tilde{p}\|_2\right), \epsilon_{\text{floor}}\right), \tag{7}$$

where $\alpha$ corresponds to a factor that sets the absolute tolerance relative to the current spectral peak for which value of $10^{-4}$ seems reasonable. The additional parameter $\epsilon_{\text{floor}}$ represents an absolute limit, for which we assume a value of $10^{-4}$ Pa m, realistic for unit point sources. This hybrid formulation ensures high precision near spectral peaks while preventing unnecessary further refinement in negligible regions. The global maximum will be dynamically updated during the sampling process as well.

### 3.3. Global convergence criterion

While the strategy proposed by Park et al. primarily focuses on the local accuracy of the wavenumber spectrum, this study introduces a global convergence criterion to serve as an additional termination condition for the refinement process.

After each refinement iteration $j$, the total integral of the complex-valued spectral magnitude is calculated using the current piecewise linear approximation $\tilde{p}_{\text{linear},j}$, which reads as

$$I_{\text{Re},j} = \int_0^{k_{z,\max}} \text{Re}\left\{\tilde{p}_{\text{linear},j}\left(k_z\right)\right\} \mathrm{d}k_z \,, \tag{8}$$

$$I_{\text{Im},j} = \int_0^{k_{z,\max}} \text{Im}\left\{\tilde{p}_{\text{linear},j}\left(k_z\right)\right\} \mathrm{d}k_z \,. \tag{9}$$

Owing to the $k_z^2$ dependency in the 2.5D Helmholtz equation (Eq. (5)), the wavenumber spectrum $\tilde{p}(k_z)$ is inherently symmetric about $k_z = 0$. Consequently, the computational effort is halved by evaluating only the positive semi-axis $[0, k_{z,\max}]$.

The refinement process is considered complete either when all linear segments meet the local stopping criterion as defined by Section 3.2 or when the relative change in both the real and imaginary integrals falls below a predefined threshold $\epsilon_{\text{tol,rel,global}}$

$$\max\left(\frac{|I_{\text{Re},j} - I_{\text{Re},j-1}|}{|I_{\text{Re},j}|}, \frac{|I_{\text{Im},j} - I_{\text{Im},j-1}|}{|I_{\text{Im},j}|}\right) \leq \epsilon_{\text{tol,rel,global}} \,. \tag{10}$$

In this study, the global tolerance is set to $10^{-3}$, i.e. refinement stops once the integrated pressure changes by less than 0.1 % between iterations, which is sufficiently accurate for practical engineering applications.

### 3.4. Filon-type quadrature

Once the adaptive sampling process is complete, the wavenumber spectrum $\tilde{p}\left(k_z\right)$ is defined by a series of piecewise linear segments. The final spatial pressure field $p\left(x, y, z\right)$ is obtained by evaluating the inverse Fourier transform (Eq. (4)). However, the presence of the complex exponential kernel $e^{-ik_z z}$ introduces high-frequency oscillations for larger spatial coordinate $z$. To ensure integration accuracy without excessively increasing the sampling density, Filon-type quadrature is employed. This method integrates the oscillatory kernel analytically against the piecewise linear approximation of the spectrum. Unlike classical quadrature, which approximates the entire integrand and therefore requires many sampling points per oscillation, only the non-oscillatory amplitude is approximated here, while its product with the oscillatory kernel is integrated in closed form (for details see, e.g.,[5]). Thus, the precision of the spatial solution depends only on the quality of the adaptive spectral approximation and the truncation of the wavenumber limit.

Due to the $k_z^2$ dependency in Eq. (5), the spectrum satisfies the symmetry condition $\tilde{p}(k_z) = \tilde{p}(-k_z)$. By analysing the parity of the integration, the integration of the complex product $\tilde{p} \cdot \left(\cos\left(k_z z\right) - i \sin\left(k_z z\right)\right)$ reveals that the sine components cancel over symmetric integration limits (*even* × *odd* = *odd*). This reduces Eq. (4) to a cosine transform over the positive semi-axis, which reads as

$$p\left(x, y, z\right) = \frac{1}{\pi} \int_0^{k_{z,\max}} \tilde{p}\left(x, y, k_z\right) \cos\left(k_z z\right) \mathrm{d}k_z \,, \tag{11}$$

where the factor $\frac{1}{\pi}$ results from the vanishing sine terms and the doubling of the cosine terms. Equation (11) is subsequently solved by expanding the complex spectrum $\tilde{p} = \mathrm{Re}\{\tilde{p}\} + i\mathrm{Im}\{\tilde{p}\}$ into two real-valued Filon-cosine integrals. Taking the real component $\mathrm{Re}\{\tilde{p}\}$ as a representative example, the analytical solution for a single linear segment $[k_{z,i}, k_{z,i+1}]$ of width $\Delta k_{z,i}$ is given by

$$\begin{aligned} I_{\mathrm{Re},i}(z) &= \int_{k_{z,i}}^{k_{z,i+1}} \mathrm{Re}\{\tilde{p}_{\mathrm{linear},i}(k_z)\} \cos(k_z z)\, dk_z \\ &= \mathrm{Re}\{\tilde{p}(k_{z,i})\} W_i^{\cos}(z, \Delta k_{z,i}) \\ &\quad + \mathrm{Re}\{\tilde{p}(k_{z,i+1})\} W_{i+1}^{\cos}(z, \Delta k_{z,i}) \,. \end{aligned} \tag{12}$$

The specific analytical weights $W_i^{\cos}$ and $W_{i+1}^{\cos}$ depend solely on the segment width $\Delta k_{z,i}$ and the spatial coordinate $z$. They are obtained by integrating the linear basis functions against the oscillatory kernel, resulting in the following explicit formulations:

$$W_i^{\cos} = -\frac{\sin(k_{z,i} z)}{z} - \frac{\cos(k_{z,i+1} z) - \cos(k_{z,i} z)}{\Delta k_{z,i} z^2} \,, \tag{13}$$

$$W_{i+1}^{\cos} = \frac{\sin(k_{z,i+1} z)}{z} + \frac{\cos(k_{z,i+1} z) - \cos(k_{z,i} z)}{\Delta k_{z,i} z^2} \,. \tag{14}$$

An identical operation is performed for the imaginary component $\mathrm{Im}\{\tilde{p}\}$, yielding $I_{\mathrm{Im},i}$. The total spatial pressure at coordinate $z$ is then reconstructed by summing the contributions from all $N$ segments across both components, yields

$$p(x, y, z) = \frac{1}{\pi} \sum_{i=0}^{N-1} \left( I_{\mathrm{Re},i}(z) + i I_{\mathrm{Im},i}(z) \right) \,. \tag{15}$$

This formulation ensures that the numerical error is decoupled from the oscillation frequency, depending only on the fidelity of the adaptive spectral approximation. Alternatively, logarithmically spaced wavenumber sampling [6] combined with a fast transform in logarithmic variables [7] allows the inverse transform to be evaluated efficiently over a broad range of $z$.

### 3.5. Robust adaptive wavenumber sampling

The proposed algorithm integrates the local and global refinement criteria from the previous sections into a single automated workflow, summarised in Algorithm 1. Starting from a coarse, equidistant sampling of the wavenumber axis, the scheme evaluates the 2.5D FE solution and then refines the grid adaptively. In each refinement loop, an interval is subdivided whenever the hybrid local error criterion is violated. Refinement continues until all intervals are resolved or the relative change of the global integrals falls below $\epsilon_{\mathrm{tol,rel,global}}$. The spatial pressure is finally recovered from the converged spectrum by evaluating the inverse Fourier transform with the composite Filon-type quadrature.

**Algorithm 1** Robust Adaptive Wavenumber Sampling Scheme

**Require:** Truncation limit $k_{z,\max}$; number of initial points $N$; relative tolerance $\epsilon_{\mathrm{tol,rel}}$; scale factor $\alpha$ and floor $\epsilon_{\mathrm{floor}}$; global tolerance $\epsilon_{\mathrm{tol,rel,global}}$; receiver coordinates $\mathbf{z}$
**Ensure:** Reconstructed spatial pressure $p(\mathbf{z})$

*Initialization: coarse sampling of wavenumber axis*

```
K ← {k_z,0, ..., k_z,N−1} equidistant on [0, k_z,max]
for all k_z ∈ K do
    p̃(k_z) ← solve 2.5D problem                    ▷ Eq. (5)
p̂_max ← max_{k_z∈K} ‖p̃(k_z)‖_2                    ▷ get maximum
(I_Re, I_Im) ← ∫ p̃_linear over K                  ▷ Eqs. (8) and (9)
```

*Adaptive refinement loop*

```
repeat
    (I_Re^prev, I_Im^prev) ← (I_Re, I_Im)          ▷ save previous
    ϵ_tol,abs ← max(α p̂_max, ϵ_floor)              ▷ Eq. (7)
    M ← ∅                          ▷ midpoints flagged for insertion
    for all intervals [k_z,i, k_z,i+1] of current K do
        k_z,m,i ← k_z,i + Δk_z,i/2                 ▷ interval midpoint
        p̃_lin ← p̃(k_z,i), p̃(k_z,i+1)               ▷ interpolation
        p̃_true ← FE solve at k_z,m,i               ▷ Eq. (5)
        p̂_max ← max(p̂_max, ‖p̃_true‖_2)            ▷ update
        if not converged then                     ▷ Section 3.2
            M ← M ∪ {(k_z,m,i, p̃_true)}
    insert every (k_z,m,i, p̃_true) ∈ M into K      ▷ subdivide flagged intervals
    (I_Re, I_Im) ← integrate p̃_linear over K       ▷ Eqs. (8) and (9)
    r_global ← max( |I_Re − I_Re^prev| / |I_Re| , |I_Im − I_Im^prev| / |I_Im| )
                              ▷ global convergence measure, Section 3.3
until M = ∅ or r_global ≤ ϵ_tol,rel,global
```

*Spatial solution reconstruction*

```
for all receiver coordinates z ∈ z do
    p(z) ← (1/π) Σ_i (I_Re,i(z) + i I_Im,i(z))     ▷ Eq. (15)
return p(z)
```

## 4. Application Example and Results

The proposed robust adaptive wavenumber sampling strategy is applied to a railway acoustics problem involving a train car body in a free-field environment, where the governing 2.5D Helmholtz equation is solved via the finite element method.

### 4.1. Model setup

The 2D finite element model represents the cross-section of a train car body within a semi-circular computational domain of 8 m radius as shown in Fig. 2. Exploiting lateral symmetry, only half of the domain is modeled. The acoustic medium is air with a speed of sound $c_0 = 343\,\mathrm{m\,s^{-1}}$. The model is excited by a monopole point source at $f_{\mathrm{exci}} = 400\,\mathrm{Hz}$ in the underfloor area. Sound hard boundary conditions are

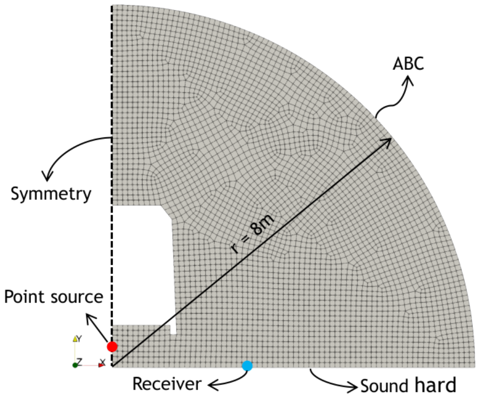


**Figure 2:** Mesh and setup of the 2.5D FE model.

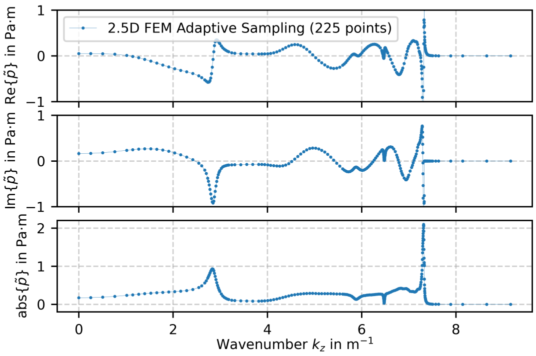


**Figure 3:** Adaptively sampled wavenumber spectrum of a representative point for an excitation frequency of 400 Hz.

applied to the ground and the symmetry plane, while the outer boundary is truncated with an absorbing boundary condition to simulate the far-field. The same mesh is used for all 2D subproblems. Its density is set to six second-order quadrilateral elements per wavelength at a reference frequency of 1000 Hz, which lies well above the excitation frequency of 400 Hz and thus provides a conservative spatial resolution. Since the effective in-plane wavelength is shortest at $k_z = 0$ and only increases for larger $k_z$, this single discretisation resolves the $k_z = 0$ subproblem and is therefore sufficient across the entire wavenumber sweep. The absorbing boundary condition is likewise independent of $k_z$ and is applied identically to every subproblem.

### 4.2. Adaptive wavenumber spectrum

Figure 3 shows the adaptively sampled complex-valued wavenumber spectrum at the receiver location marked in Fig. 2. The sampling density increases around the excitation frequency, where the spectrum exhibits a singularity, as well as in regions where the real and imaginary parts show high-gradient fluctuations. The local amplitude maximum near $k_z \approx 2.8\,\mathrm{m}^{-1}$ is caused by an acoustic resonance in the underfloor area between the car body and the ground. In contrast, regions with low gradients are sampled sparsely. For instance, the range from $0\,\mathrm{m}^{-1}$ to $2.5\,\mathrm{m}^{-1}$ is represented by a coarse discretisation. The effectiveness of the hybrid error metric is most evident in the evanescent region. Despite the rapid decay of the spectrum amplitude and the choice of a high upper wavenumber

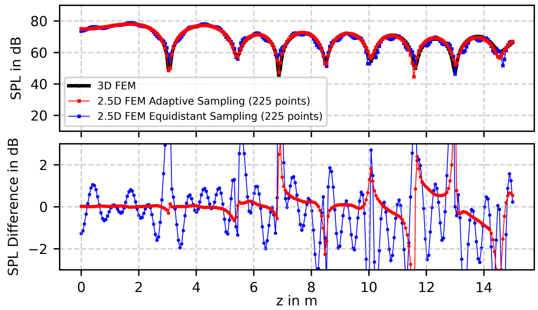


**Figure 4:** Axial sound pressure level (SPL) distribution at the receiver location (top) and difference of 2.5D results with respect to the 3D reference (bottom).

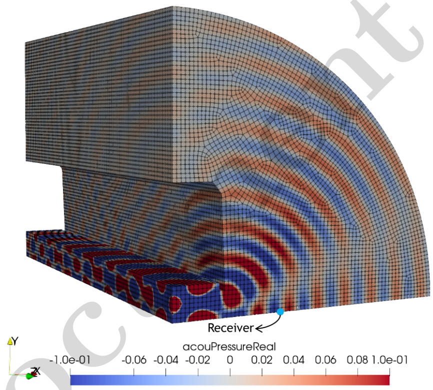


**Figure 5:** Pressure result from the 3D FEM model.

limit, the refinement process remains stable. The absolute tolerance floor prevents unnecessary sampling in this area, where the amplitude approaches zero. Consequently, only a few points are required to represent the decaying tail, increasing computational efficiency.

### 4.3. Spatial pressure results

The axial sound pressure distribution at the receiver point is shown in Fig. 4. A 3D finite element model with a length of 15 m serves as the reference solution, the result of which is illustrated in Fig. 5. Due to computational constraints, the 3D domain is truncated at 15 m with perfectly matched layers, whereas the 2.5D model assumes an infinitely long domain in the axial direction. Two 2.5D solutions are compared: one utilising the proposed adaptive sampling strategy (red) and the other using equidistant sampling (blue). Both methods share the same number of wavenumber steps to ensure a fair comparison of efficiency. The difference in sound pressure level relative to the 3D reference is also computed. The results indicate that the adaptively sampled 2.5D solution is more consistent with the reference than the equidistantly sampled one. This improved agreement is most pronounced at the maxima of the sound pressure level, where the deviation from the 3D reference is smallest. These high-amplitude regions are the most relevant ones, as they dominate the total radiated sound power and the perceived loudness. Deviations occurring in regions of low sound pressure level, in contrast, contribute negligibly to the overall energy balance and are therefore of minor practical importance.

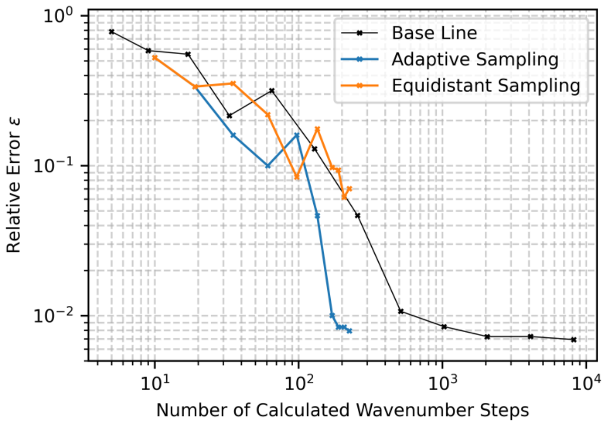


**Figure 6:** Comparison of convergence rate using different wavenumber sampling strategies: A baseline of progressive equidistant refinements from 5 initial points (black), the proposed adaptive strategy starting with 10 initial steps (blue), and a fixed-step equidistant sampling using a point count equivalent to each adaptive iteration (orange).

### 4.4. Convergence rate

To quantitatively evaluate the performance of the proposed adaptive sampling strategy, the relative error is calculated between the 3D FEM reference vector and the reconstructed 2.5D solutions at all nodal coordinates. The resulting convergence rate as a function of the number of calculated wavenumber steps is shown in Fig. 6. The adaptive strategy converges significantly faster than both equidistant approaches, reaching a relative error of $10^{-2}$ with substantially fewer wavenumber evaluations. This higher accuracy per iteration confirms that the adaptive refinement of the wavenumber spectrum is more computationally efficient than uniform discretisation. The adaptive process terminates automatically once the predefined convergence criteria are satisfied, ensuring a robust balance between numerical precision and computational effort. Although the comparison above is expressed in terms of the number of wavenumber evaluations, this measure directly reflects the computational cost, since each evaluation requires one 2D finite element solve, whereas the subsequent Filon-type reconstruction and the adaptive bookkeeping are negligible in comparison. For the present model, a single 2D solve takes approximately 0.2 s, so that the adaptive strategy with 225 evaluations amounts to about 45 s, compared to roughly 200 s for the 1000 evaluations required by the equidistant baseline to reach a comparable accuracy. The relative saving is independent of the hardware, as the cost per solve enters both cases identically.

## 5. Conclusion

The proposed adaptive wavenumber sampling has been applied to a representative application example of a railway car body in a free field. The obtained 2.5D acoustic solution was found to be accurate as compared to a reference 3D computation. Comparing the novel adaptive sampling strategy with a traditional equidistant sampling showed significantly higher convergence rates, allowing for obtaining equivalent global accuracy in the pressure field with a significantly lower number of costly evaluations of the 2.5D wavenumber problems. A further advantage of the proposed algorithm is its automatic termination based on predefined error measures. It is expected that these error measures can be related to the accuracy of the 2.5D solution compared to a reference 3D solution. In an upcoming study, we will also investigate whether the proposed adaptive sampling strategy is equally effective for tunnel-like configurations, where the wavenumber spectrum is dominated by peaks arising from the acoustical modes of the cross-section.

## 6. Acknowledgments

This work was partly funded by the Austrian Research Promotion Agency (FFG) within the program line "Bridge" (project number 55551190).

## References

[1] C. H. Kasess, T. Maly, W. Kreuzer, and H. Waubke, "The effect of reflecting panels on the efficiency of railway noise barriers," *The Journal of the Acoustical Society of America*, vol. 157, no. 5, pp. 3718–3729, 2025, ISSN: 0001-4966. DOI: 10.1121/10.0036697.

[2] H. Li, D. Thompson, and G. Squicciarini, "A 2.5D acoustic finite element method applied to railway acoustics," *Applied Acoustics*, vol. 182, p. 108 270, Nov. 2021, ISSN: 0003-682X. DOI: 10.1016/j.apacoust.2021.108270.

[3] J. Park, K. Norén-Cosgriff, and A. M. Kaynia, "Numerical wavenumber integration for 2.5d wave equation solution," in *XI International Conference on Structural Dynamics*, ser. EURODYN 2020, EASD, 2020, pp. 2919–2925. DOI: 10.47964/1120.9239.19610.

[4] D. Duhamel, "Efficient calculation of the three-dimensional sound pressure field around a noise barrier," *Journal of Sound and Vibration*, vol. 197, no. 5, pp. 547–571, Nov. 1996, ISSN: 0022-460X. DOI: 10.1006/jsvi.1996.0548.

[5] A. Iserles and S. P. NØrsett, "On Quadrature Methods for Highly Oscillatory Integrals and Their Implementation," *BIT Numerical Mathematics*, vol. 44, no. 4, pp. 755–772, 2004, ISSN: 1572-9125. DOI: 10.1007/s10543-004-5243-3.

[6] J. Fakhraei, R. Arcos, T. Pàmies, and J. Romeu, "2.5D singular boundary method for exterior acoustic radiation and scattering problems," *Engineering Analysis with Boundary Elements*, vol. 143, pp. 293–304, 2022, ISSN: 0955-7997. DOI: 10.1016/j.enganabound.2022.06.017.

[7] J. D. Talman, "Numerical Fourier and Bessel transforms in logarithmic variables," *Journal of Computational Physics*, vol. 29, no. 1, pp. 35–48, 1978, ISSN: 0021-9991. DOI: 10.1016/0021-9991(78)90107-9.